Using Hyperspectral Crop Residue Angle Index to Estimate Maize and Winter-Wheat Residue Cover: A Laboratory Study

Jibo Yue [1,2,3], Qingjiu Tian [1,2,*], Xinyu Dong [1,2], Kaijian Xu [1,2] and Chengquan Zhou [3,4]

[1] International Institute for Earth System Science, Nanjing University, Nanjing 210023, China; yuejb.ha@gmail.com or dg1727034@smail.nju.edu.cn (J.Y.); dg1827003@smail.nju.edu.cn (X.D.); dg1627024@smail.nju.edu.cn (K.X.)

[2] Jiangsu Provincial Key Laboratory of Geographic Information Science and Technology, Nanjing University, Nanjing 210023, China

[3] Key Laboratory of Quantitative Remote Sensing in Agriculture of Ministry of Agriculture China, Beijing Research Center for Information Technology in Agriculture, Beijing 100097, China; zhoucq@zaas.ac.cn

[4] Institute of Digital Agriculture, Zhejiang Academy of Agricultural Sciences, Hangzhou 310021, China

* Correspondence: tianqj@nju.edu.cn; Tel.: +86-(25)-89687317

check for
updates

Abstract: Crop residue left in the field after harvest helps to protect against water and wind erosion, increase soil organic matter, and improve soil quality, so a proper estimate of the quantity of crop residue is crucial to optimize tillage and for research into environmental effects. Although remote-sensing-based techniques to estimate crop residue cover (CRC) have proven to be good tools for determining CRC, their application is limited by variations in the moisture of crop residue and soil. In this study, we propose a crop residue angle index (CRAI) to estimate the CRC for four distinct soils with varying soil moisture (SM) content and crop residue moisture (CRM). The current study uses laboratory-based tests ((i) a dry dataset (air-dried soils and crop residues, $n = 392$); (ii) a wet dataset (wet soils and crop residues, $n = 822$); (iii) a saturated dataset (saturated soils and crop residues, $n = 402$); and (iv) all datasets ($n = 1616$)), which allows us to analysis the soil and crop residue hyperspectral response to varying SM/CRM. The CRAI combines two features that reflect the moisture content in soil and crop residue. The first is the different reflectance of soil and crop residue as a function of moisture in the near-infrared band (833 nm) and short-wave near-infrared band (1670 nm), and the second is different reflectance of soils and crop residues to lignin, cellulose, and moisture in the bands at 2101, 2031, and 2201 nm. The effects of moisture and soil type on the proposed CRAI and selected traditional spectral indices ((i) hyperspectral cellulose absorption index; (ii) hyperspectral shortwave infrared normalized difference residue index; and (iii) selected broad-band spectral indices) were compared by using a laboratory-based dataset. The results show that the SM/CRM significantly affects the broad-band spectral indices and all other spectral indices investigated are less correlated with CRC when using all datasets than when using only the dry, wet, or saturated dataset. Laboratory study suggests that the CRAI is promising for estimating CRC with the four soils and with varying SM/CRM. However, because the CRAI was only validated by a laboratory-based dataset, additional field testing is thus required to verify the use of satellite hyperspectral remote-sensing images for different crops and ecological areas.

Keywords: crop residue cover; crop residue moisture; soil moisture; angle index; remote sensing

1. Introduction

Crop residue left in the field after harvest helps protect against water and wind erosion, increase soil organic matter, and improve soil quality [1–3]. Because tillage intensity is the main management lever for controlling crop residue cover (CRC), a reduction in tillage is associated with increasing soil organic matter and water retention [2,4]. The decomposition and burning of crop residue produces carbon dioxide (CO_2) and other gases, increasing atmospheric carbon [4,5]. Thus, the proper management of crop residue is an integral part of many eco-friendly tillage systems and a major focus of research into the environmental effects of agricultural practices [6–8].

Prior to the emergence of remote-sensing technology, large CRC surveys were limited by labor and resources. To date, the two traditional methods of line-point transect and photography have been used to measure the field CRC [9,10]. However, manual survey-based methods for quantifying CRC are time- and labor-consuming and, more importantly, are difficult to apply over large areas. In recent decades, spectral remote-sensing data acquired from ground platforms, unmanned aerial vehicles, airborne platforms, and satellite platforms have been used to capture field spectra in narrow bands and have provided information about the soil surface. As a result, tillage practices and estimating CRC based on remote-sensing data has become a topic of significant interest to environmental and agricultural researchers [11–17].

Crop-residue reflectance spectra depend on crop type, variety, moisture content, lignin and cellulose content, and other factors [18–23]. Soil and crop residues have different spectral absorption features and therefore different spectral reflectance features [5,23–26]. In recent years, a series of methods to estimate CRC based on remote-sensing data has been proposed and applied on local and regional scales to monitor crop residue. These methods may be divided into three types: (i) the linear spectral unmixing technique, (ii) the spectral index (SI) technique, and (iii) the triangle space technique. Linear spectral unmixing is a physical model that determines the relative contribution or abundance of each endmember relative to the total reflectance recorded for each pixel [27]. The output of spectral unmixing is a series of fraction maps that indicates the proportion (range 0 to 1) of each endmember present in each pixel [28]. Linear spectral unmixing can be applied to multispectral remote-sensing data only if reflectance is determined by a limited number of endmembers, such as soil and crop residue [29]. The SI technique has achieved great success in remote-sensing-based farmland monitoring. An SI is a combination of two or more remotely detected reflectance bands. Estimates of CRC based on remote-sensing data are quantified by using SIs, such as the dead fuel index (DFI) [30], the normalized difference index (NDI, NDI5, and NDI7) [31], the normalized difference tillage index [32], the normalized difference senescent vegetation index (NDSVI) [33], the short-wave near-infrared normalized difference residue index (SRNDI) [34], the cellulose absorption index (CAI) [35], the shortwave infrared normalized difference residue index (SINDRI) [36], and lignin cellulose absorption [37]. A linear or exponential empirical CRC-estimation equation can be constructed and applied to remote-sensing data by using SI methods. The triangle-space technique uses two SIs or bands to create a two-dimensional scatter map, as done in the methods involving the multiband crop-residue index [38] or the CAI normalized difference vegetation index [39]. This approach determines the proportions of crop residue, soil, and vegetation on the soil surface based on their spatial locations in a triangular space.

However, the use of remote-sensing-based techniques to estimate CRC has been limited by the variations in the field of moisture in the crop residue and soil [18,20,23]. Variations in the distribution of crop residue moisture (CRM) and of soil moisture (SM) in the field lead to variations in each pixel of the endmember spectra of crop residue and soil [24,40]. For example, in practice, linear spectral unmixing techniques that use fixed crop residue and soil endmember spectra can lead to inaccurate estimates of the spectral constituents that indicate the abundance of pure crop residue [41]. In addition, the cellulose and lignin absorption features are attenuated as moisture content increases, thereby reducing the accuracy of estimates of CRC based on existing SIs [20,24]. Thus, an accurate estimate of CRC requires consideration of the moisture distribution in the field.

A laboratory-based hyperspectral analysis that takes into account SM/CRM effects is very meaningful to estimation of CRC accurately. The current study uses laboratory-based tests ((i) a dry dataset (air-dried soils and crop residues, n = 392); (ii) a wet dataset (wet soils and crop residues, n = 822); (iii) a saturated dataset (saturated soils and crop residues, n = 402); and (iv) all datasets (n = 1616)), which allows us to analysis the soil and crop residue hyperspectral response to varying SM/CRM. The present study proposes a crop residue angle index (CRAI) to estimate the CRC for four distinct soils, various SM/CRM. The CRAI combines two features that reflect the moisture content of soils and crop residue (Section 2.2). The first is the that the moisture content of soil and crop residue causes differing reflectance in the near-infrared band (833 nm) and the short-wave near-infrared band (SWIR, 1670 nm), and the second is that the lignin, cellulose, and moisture content of soil and crop residue causes differing reflectance in the bands at 2101, 2031, and 2201 nm. Laboratory study suggests that the CRAI is promising for estimating CRC with the four soils and with varying SM/CRM. (Note that the CRAI has yet to be verified in the field). The method involves the following three steps:

(1) Spectral data from laboratory measurements (dry, wet, and saturated samples) are used to analyze the soils/crop residues hyperspectral response to SM/CRM (Section 2.1), and crop residue angle index to combine two hyperspectral angle features (Section 2.2).

(2) Spectral data from laboratory measurements are used to analyze the correlation coefficients between CRC and (i) nine broad-band SIs, (ii) the SINDRI, and (iii) the CAI (Section 4.1).

(3) Spectral data from laboratory measurements are used to analyze the response of SIs to SM/CRM and soil background. Laboratory-based (i) dry, (ii) wet, (iii) saturated, and (iv) all datasets are used to compare how moisture content and soil background affect the selected SIs ((i) the proposed CRAI, (ii) the CAI, (iii) the SINDRI, and (iv) selected broad-band-based Sis) (Section 4.2).

(4) Random sampling validation is used to evaluate the accuracy of estimates of CRC based on these SIs (Section 4.3). We also discuss the accuracy of CRC estimates based on SIs (Section 5).

2. Background and Proposed Crop Residue Angle Index

2.1. Response to Moisture of Crop Residue and Soil Reflectance

Soil reflectance is affected by intrinsic soil factors: SM, amount of organic matter, particle-size distribution, mineral composition, and color of soil elements [42–44]. Soil reflectance decreases as the SM increases, primarily because changing the medium surrounding soil particles from air to water decreases their relative refractive index, thus increasing the average degree of forward scattering as determined by the asymmetry parameter (i.e., the mean cosine of the scattering angle) [45]. Figure 1 shows the mean reflectance spectra of four soils (dry and wet).
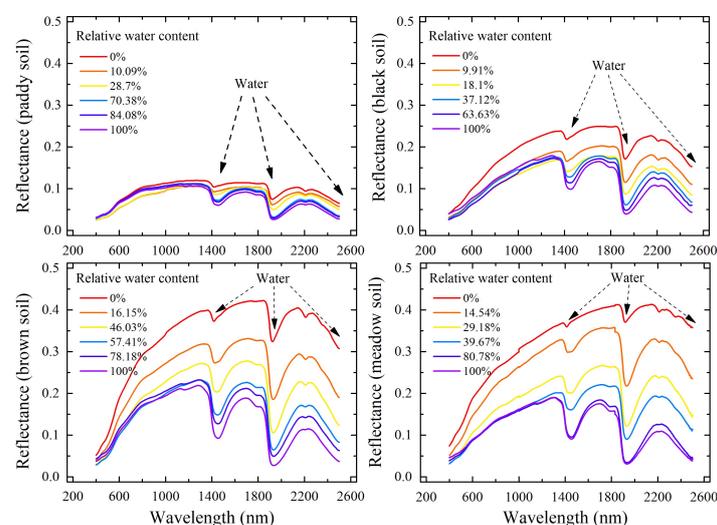
Figure 1. Reflectance spectra (400–2500 nm) of four distinct soils with different relative water contents.

Figure 2 shows the mean reflectance spectra of maize and winter-wheat residue (dry and wet). Hyperspectral data in this work was collected by using an ASD (Analytical Spectral Devices, Boulder, USA) FieldSpec 3 spectrometer. Moisture more strongly affects crop residue reflectance in the SWIR region (1100–2500 nm) than in the visible region (350–800 nm) because of the strong water absorption bands in the SWIR [46]. As CRM increases, the mean crop residue reflectance spectra remain nearly constant in the visible range. However, the reflectance spectra are significantly attenuated in the near-infrared (NIR) and SWIR. As CRM increases, two water absorption bands (one centered at 1450 nm and one centered at 1950 nm) become dominant in the SWIR (Figure 2), which is consistent with the findings of Wang [23] and Daughtry [22].
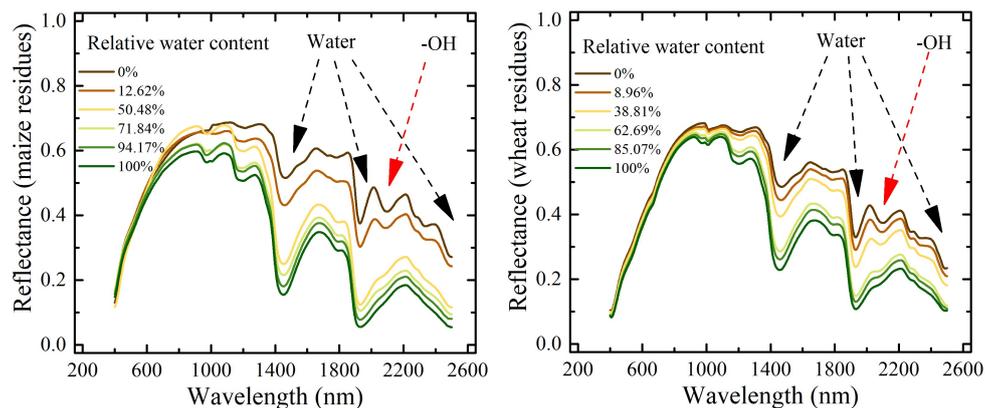
Figure 2. Reflectance spectra (400–2500 nm) of two crop residues with different relative water contents.

Daughtry et al. [20,22] suggested that the absorption features near 2100 nm are probably associated with lignin and cellulose in crop residue and these features are also evident in the reflectance spectra of all dry crop residue. However, the features indicative of lignin and cellulose (absorption features near 2100 nm) gradually disappear (see Figure 2) as the relative water content increases [21,29]. The hyperspectral reflectance for wet and dry crop residue (maize and winter wheat) in Figure 2 indicate that the sensitivity of the absorption features (bands from 2000 to 2200 nm) could be weakened by water absorption [22,23,47]. Therefore, the use of remote-sensing-based techniques to estimate CRC are limited by variations in the field of moisture in crop residue and soil.

2.2. Proposed Crop Residue Angle Index and Its Response to Moisture

In this study, we propose a CRAI to estimate CRC from four types of soil with varying SM/CRM. The CRAI combines two features that reflect the moisture of the soil and crop residue. The first is that variations in moisture content in soil and crop residue causes differing reflectance in the near-infrared band (833 nm) and in the SWIR band (1670 nm; expressed in terms of the angle α in Figure 3a,c), and the second is that the lignin, cellulose, and moisture content of soil and crop residue causes differing reflectance in the bands at 2101, 2031, and 2201 nm (expressed in terms of the angle β in Figure 3b,d). The angles α and β are defined in Figure 3. The angle α is the included angle between the vertical direction and the line from the near-infrared reflectance (833 nm in this work) to the SWIR reflectance (1670 nm in this work). The angle β is the included angle between (i) the line from the reflectance at 2101 nm to the reflectance at 2031 nm and (ii) the line from the reflectance at 2101 nm to the reflectance at 2201 nm. As shown in Figure 3, both the soil and the crop residue reflectance decrease as SM increases, and the two water-absorption bands centered at 1450 and 1950 nm become dominant in the SWIR bands. The reflectance in the SWIR bands of both the soil and crop (wheat) residue reflectance decrease faster than in the NIR region because the water absorption more strongly affects the SWIR bands (1670 nm) than the NIR bands (833 nm). The results shown in Figure 3a,c,e indicate that the angle α both for soil and for wheat residue increases with SM and CRM. Figure 3a,c also show that the variations in reflectance decrease in the NIR band as the SM/CRM increase. The different

reflectance for soil and crop residue as a function of moisture is reflected in the rapidly increase in the angle α for wheat residue as a function of CRM than for the angle α for soil (Figure 3e). In addition, the lignin and cellulose absorption features of crop residue (bands at 2031, 2101, and 2201 nm; see Daughtry et al. [20,22]) gradually disappear with increasing CRM (Figure 3d), so that the angle β for wheat residue increases with CRM (Figure 3e). Conversely, the angle β for soil is relatively constant as a function of SM (Figure 3e).
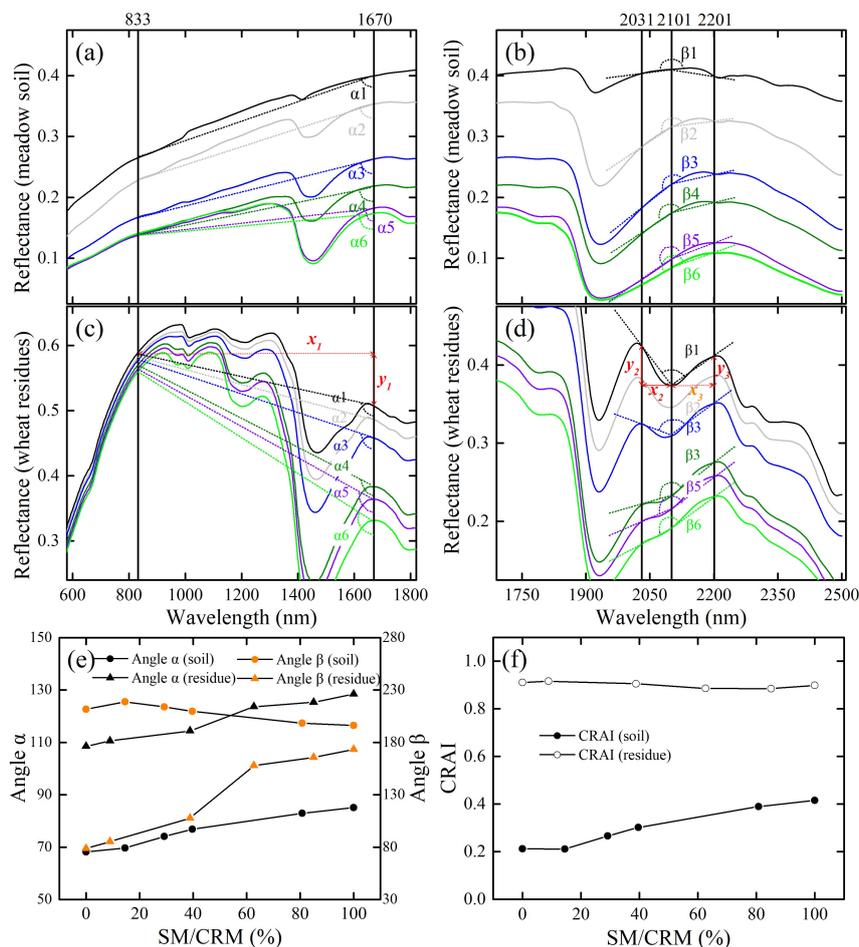
Figure 3. Angles α and β as a function of crop residue moisture and soil moisture content (same hyperspectral data as shown in Figures 1 and 2).

Figure 3a,c,e show the angle α response to the increase SM/CRM, Figure 3b,d,e show the angle β response to increase SM/CRM. Thus, as shown in Figure 3e, the reflectance as a function of moisture content of the soil and crop residue can be described by the angles α and β, which in turn may be used to construct the CRAI (Figure 3f) as follows:

$$CRAI = (angle\ \alpha - angle\ \beta / f)/100, f = 4.5. \tag{1}$$

Note that the factor $f = 4.5$ is an empirical parameter used to combine two angles. Based on 100 cycles of rough modeling and verification (with $f = 0.1$ to 10 in steps of 0.1), we find that $f = 4.5$ gives the largest correlation coefficient between CRC and CRAI. In this work, the angles α and β are calculated as follows (see Figure 3c,d):

$$Angle\ \alpha = \text{atan}(x1/y1),$$
$$x1 = wav(1670 - 833), y1 = Ref_{1670} - Ref_{833} \tag{2}$$

$$
\begin{aligned}
Angle\ \beta &= \ 180 - atan(x2/y2) - atan(x3/y3) \\
x2 &= wav(2101-2031), y2 = Ref_{2031} - Ref_{2101} \\
x3 &= wav(2201-2101), y3 = Ref_{2201} - Ref_{2101}
\end{aligned}
\tag{3}
$$

$$
wav(b1-b2) = \ (b1-b2)/2500,
\tag{4}
$$

where Ref_{833}, Ref_{1670}, Ref_{2031}, Ref_{2101}, and Ref_{2201} are the reflectance at 833, 1670, 2031, 2101, and 2201 nm, respectively, and wav (1670–833), wav (2101–2031), and wav (2201–2101) are the normalized distance from (i) 1670 to 833 nm, (ii) 2101 to 2301 nm, and (iii) 2201 to 2101 nm (calculated by using Equation (4)).

2.3. Traditional Crop Residue Cover Spectral Indices

Previous studies have proposed numerous indices to estimate CRC. Table 1 lists several promising spectral-based indices for CRC, such as the simple tillage index (STI) [32], the SRNDI [34], the NDSVI [33], DFI [30], the normalized difference tillage index (NDTI) [32], and the hyperspectral CAI [20]. The hyperspectral SINDRI is calculated from the: (i) hyperspectral bands 2210 and 2260 nm [36], (ii) ASTER SWIR bands 6 and 7 [36], and (iii) from the currently functional Worldview-3 SWIR bands 6 and 7 [14]. In addition, the shortwave green normalized difference index (SGNDI) combines Landsat-TM/OLI7 and OLI3 in this study. Table 1 shows the traditional CRC SIs from previous research.

Table 1. Spectral indices used in previous research for estimating crop residue cover.

Type	Spectral Indices	Equation	Reference
Broad-band	SGNDI	(OLI3 - OLI7)/ (OLI3 + OLI7),	This paper
	STI	OLI6/OLI7,	[32]
	MCRC	(OLI6 - OLI3)/ (OLI6 + OLI3),	[48]
	SRNDI	(OLI7 - OLI4)/ (OLI7 + OLI4),	[34]
	DFI	$100 \times (1 - OLI7/OLI6)/ (OLI4/OLI5)$,	[30]
	NDI5	(OLI5 - OLI6)/ (OLI5 + OLI6),	[31]
	NDI7	(OLI5 - OLI7)/ (OLI5 + OLI7),	[31]
	NDTI	(OLI6 - OLI7)/ (OLI6 + OLI7),	[32]
	NDSVI	(OLI6 - OLI4)/ (OLI6 + OLI4),	[33]
Hyperspectral	SINDRI	$100 \times (R_{2210} - R_{2260})/(R_{2210} + R_{2260})$ $100 \times (A6 - A7)/(A6 + A7)$,	[36]
	CAI	$100 \times ((R_{2031}+R_{2201})/2 - R_{2101})$,	[35]

Note: OLI2 (0.450–0.515 μm), OLI3 (0.525–0.600 μm), OLI4 (0.630–0.680 μm), OLI5 (0.845–0.885 μm), OLI6 (1.560–1.660 μm), and OLI7 (2.100–2.300 μm) represents broad-band multispectral of blue, green, red, near-infrared, SWIR1, and SWIR2 (e.g., Landsat-8 OLI bands 2–7, and corresponding Landsat TM and ETM+ bands 1–5 and 7). A6 (2.185–2.225 μm) and A7 (2.235–2.285 μm) represents ASTER/Worldview-3 SWIR band6 and SWIR band7. R_{2031}, R_{2101}, R_{2201}, R_{2210}, and R_{2260} represents bands at 2031, 2101, 2201, 2210, and 2260 nm of hyperspectral reflectance, respectively.

3. Laboratory Data Collection

Two crop residues (winter wheat and maize) and four spectrally distinct soils (paddy soil, black soil, meadow soil, and brown soil; see details in Table A1) were collected from fields (soil reflectance spectra are shown in Figure 1, crop residue reflectance spectra are shown in Figure 2) in Jining City and Nanjing City (Table A1). Jining City has a medium-latitude monsoon climate, an average rainfall of 751 mm, and an average temperature of 13.6 °C. (Meteorological data were acquired from the China Meteorological Data Service, http://data.cma.cn/). Winter wheat, maize and soya bean are the main crops in Jining. Winter-wheat residue was collected in Jining City (harvested in early June, 2018). Nanjing City has an average altitude of 20 m, a subtropical humid monsoon climate, an average rainfall of 1106 mm, and an average temperature of 15.4 °C. Maize, winter wheat, and rice are the main crops in Nanjing. Maize residue was collected in Nanjing City (harvested at the end of October, 2018).

The soil texture was analyzed, and the percentage of clay, silt, and sand in soil samples was calculated. Table A1 summarizes the characteristics of the field soil and shows that the soils texture is clay.

3.1. Laboratory Measurements

3.1.1. Hyperspectral Measurements

In a spectral laboratory, we measured the dry, wet, and saturated soils and the crop residue mixed hyperspectral reflectance by using an ASD FieldSpec 3 spectrometer (see Figure 4). The ASD FieldSpec 3 spectrometer offers full-range detection (350–2500 nm with a spectral resolution of 3 nm at 700 nm, 8.5 nm at 1400 nm, and 6.5 nm at 2100 nm) and acquires visible/NIR/SWIR data over the entire solar spectrum. In addition, the data were automatically resampled for 1 nm spacing. As shown in Figure 4, all samples were illuminated by a halogen lamp mounted on the arm of a camera stand and held 50 cm above the workbench to create a 45° illumination zenith angle. The bench was covered with a black tablecloth. The field spectrometer was calibrated by using the reflectance from a 40×40 cm $BaSO_4$ reference panel, and the hyperspectral reflectance of each sample was acquired with the ASD FieldSpec 3 spectrometer fore-optic at 40 cm above the sample at a 0° zenith angle, resulting in a 0.177 m diameter field of view. Five reflectance spectra were acquired from each sample, the average of which was recorded as the reflectance spectrum for the sample.
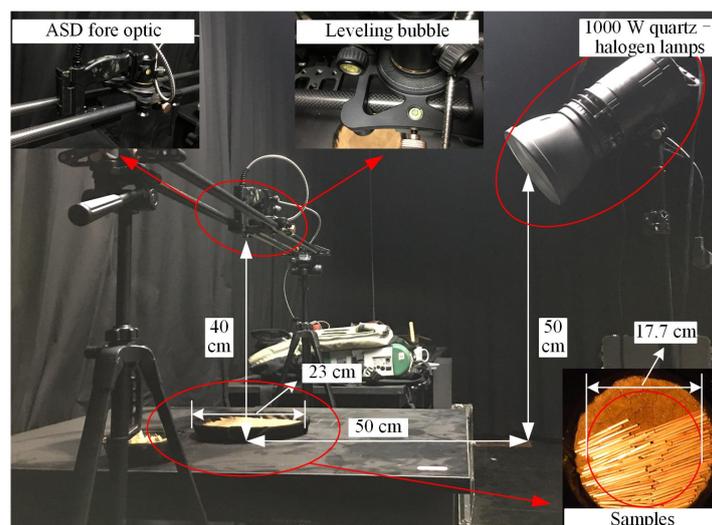
Figure 4. Experimental apparatus for measuring hyperspectral reflectance in the laboratory.

The experimental process was as follows: (i) The four soils (Table A1) were air-dried, crushed, and passed through a 2 mm screen, and then deposited to a depth of 1 cm in a round 23-cm-radius tray. The crop residue samples (air-dried) were then cut into 10 cm sections; (ii) Beginning with the bare dry soils, dry crop residue segments were gradually added onto the soil surface in the round trays. We then measured the mixed hyperspectral reflectance of the soils and crop residue and took digital photographs. When the soils were all covered by crop residue, we started to remove the crop residue sections until bare soil was reached; (iii) The crop residue samples were then placed in a round black plastic bowl and sprayed with water, and the soils were sprayed with water until saturated. As in step (ii), we then measured the mixed hyperspectral reflectance of the soils and crop residue and took digital photographs; and (iv) The saturated soil and crop residue samples were then placed in a dark room at about 24 °C for 6 and 12 hours, following which we again measured the hyperspectral reflectance of the (wet) soil and (wet) crop residue. Because crop residue was added manually, the number of samples in the various groups ranged from 43 to 56 (see Table 2).

The hyperspectral reflectance acquired in the spectroscopy laboratory was resampled to generate broad-band multispectral remote-sensing data (see Table 1) by using the corresponding spectral

response functions, which were obtained from the spectral laboratory tools available in the ENVI image-processing and analysis software (ITT Visual Information Solutions, Boulder, CO, USA).

3.1.2. Crop Residue Cover and Moisture Measurements

We used a digital camera (Canon SX710 HS, Canon Inc., Tokyo, Japan) to take top-view photographs of each sampling position. The crop residue and soil fractions in the field of view of the spectrometer were visually analyzed by using a 125 dot overlay [22] on the digital image (Figure 5). Next, the CRC was calculated by using:

$$CRC = \frac{SUM_{residue}}{125} \times 100\%,$$ (5)

where $SUM_{residue}$ is the total number of crop residue dots obtained by manual counting.
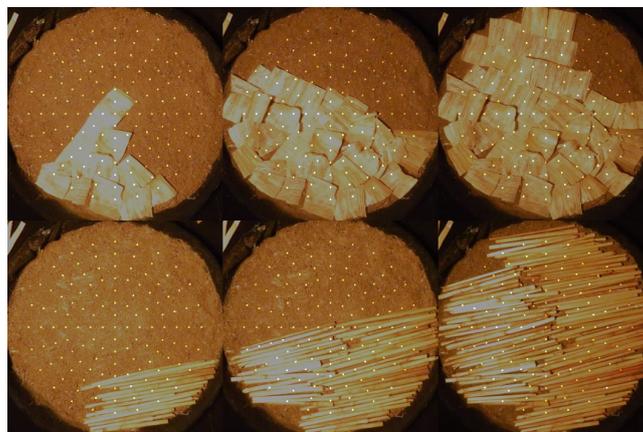
Figure 5. Digital photographs for determining crop residue cover (125 dot in 23-cm-radius tray).

In this study, the relative SM/CRM were calculated by using:

$$SM/CRM = \frac{m_0 - m_{dry}}{m_{sat} - m_{dry}},$$ (6)

where m_{sat} (m_{dry}) is the mass of saturated (air-dried) soil or crop residue sample, and m_0 is the mass of the soil or crop residue sample.

3.2. Estimate of Crop Residue Cover and Statistical Analysis

3.2.1. Estimate of Crop Residue Cover

Triangle-space techniques (e.g., DFI-NDVI [16], CAI-NDVI [39].) are widely used to estimate cropland CRC because crops and vegetation both appear in remote-sensing images. Thus, linear spectral unmixing is used to estimate the proportions of crop residue, soil, and vegetation, which makes it essential to evaluate the linear-equation-based CRC performance. In this study, we used a linear model (formula: CRC = a × Index + b) to estimate the wheat and maize CRC. From the laboratory measurements, we acquired a total of 1616 (835 for wheat, 781 for maize) sets of residues, soil hyperspectral reflectance measurements, and CRCs. Table 2 gives the descriptive statistics for the measurements of SM/CRM content.

Table 2. Descriptive statistics of average relative soil moisture (SM, %) and crop residue moisture (CRM, %) in this study.

Soils	Groups		Maize			Wheat		
			Samples	SM	CRM	Samples	SM	CRM
Brown soil	Dry		44	0	0	43	0	0
	Wet	Wet2	48	12.1	20.0	54	12.1	50.0
		Wet1	52	34.3	35.0	54	34.3	86.1
	Saturated		46	100	100	46	100	100
Black Soil	Dry		53	0	0	53	0	0
	Wet	Wet2	53	20.3	18.5	56	20.3	13.7
		Wet1	48	66.6	52.2	54	66.6	40.2
	Saturated		52	100	100	58	100	100
Meadow Soil	Dry		52	0	0	53	0	0
	Wet	Wet2	53	17.9	18.5	50	17.9	13.7
		Wet1	46	45.5	52.2	53	45.5	40.2
	Saturated		46	100	100	55	100	100
Paddy Soil	Dry		46	0	0	48	0	0
	Wet	Wet2	47	13.2	20.0	55	13.2	50.0
		Wet1	49	54.3	35.0	50	54.3	86.1
	Saturated		46	100	100	53	100	100
	Total		781			835		

Note: Dry represent air-dry soils and air-dry crop residue samples; Saturated represent saturated samples; Wet represent wet soils and wet crop residue samples, Wet1, and Wet2 represent data measured after 6, and 12 hours after saturated samples measurement. SM represent soil moisture; CRM represent crop residue moisture.

We used random sampling from all 1616 samples to evaluate the performance of the proposed CRAI and other SIs. Of these random samples, one third of the dataset (279 wheat and 261 maize) were used to analyze the relationship between the spectral indices, and the CRC. The equations for estimating the CRC from the indices were then established, and the remaining two thirds of the datasets (556 wheat and 520 maize) were used for validation.

3.2.2. Statistical Analysis

The coefficient of determination (R^2), root mean square error (RMSE), normalized root mean square error (nRMSE), and mean absolute error (MAE) were used to evaluate the performance of each model. Mathematically, a higher R^2 corresponds to a smaller RMSE and MAE, and thus indicates a more accurate model. The following equations were used to calculate R^2, RMSE, nRMSE, and MAE:

$$R^2 = 1 - \frac{\sum_{i=1}^{n}(y_i - x_i)^2}{\sum_{i=1}^{n}(y_i - \overline{y})^2}, \tag{7}$$

$$\text{RMSE} = \sqrt{\frac{\sum\limits_{i=1}^{n}(x_i - y_i)^2}{n}}, \tag{8}$$

$$\text{nRMSE} = \frac{RMSE}{y_{\max} - y_{\min}}, \tag{9}$$

$$\text{MAE} = \frac{\sum\limits_{i=1}^{n}|x_i - y_i|}{n}, \tag{10}$$

where x_i and y_i are the estimated and measured values, respectively, $\overline{x}$ and $\overline{y}$ are the average estimated and measured values, respectively, n is the sample number, and y_{max} and y_{min} are the measured maximum and minimum CRC, respectively.

4. Results

4.1. Selection of Traditional Broad-Band Spectral Indices

Table 3 shows the correlation coefficients *r* between the CRC and the eleven investigated crop residue indices from laboratory hyperspectral. The results show that all the measured indices are correlated to varying degrees with the CRC. Table 3 ranks the traditional broad-band indices according to the absolute value of the correlation coefficient. Of the nine traditional broad-band indices investigated, the SGNDI leads to the most accurate estimates of CRC for both the (i) dry (*r* = 0.842) and (ii) wet (*r* = 0.787) datasets, whereas the NDSVI leads to the most accurate estimates of CRC (*r* = 0.757) for the saturated dataset. However, the traditional broad-band indices all have a lower correlation coefficient when using all datasets (Table 3), which means that the SM/CRM content strongly affects the traditional broad-band indices (analyzed in Section 4.2).

Table 3. Analysis of correlation between crop residue cover and crop residue indices (all dataset).

| Ranking | Samples and Dataset | | | | | | | |
| | Dry (n = 392) | | Wet (n = 822) | | Saturated (n = 402) | | All (n = 1616) | |
	Indices	$\lvert r \rvert$	Indices	$\lvert r \rvert$	Indices	$\lvert r \rvert$	Indices	$\lvert r \rvert$
1	SGNDI	0.842[**]	SGNDI	0.787[**]	NDSVI	0.856[**]	NDSVI	0.685[**]
2	SRNDI	0.833[**]	SRNDI	0.787[**]	SRNDI	0.827[**]	MCRC	0.658[**]
3	DFI	0.775[**]	NDSVI	0.786[**]	SGNDI	0.81[**]	SGNDI	0.653[**]
4	NDSVI	0.768[**]	MCRC	0.704[**]	MCRC	0.741[**]	SRNDI	0.629[**]
5	NDI7	0.744[**]	NDI5	0.677[**]	NDI5	0.698[**]	NDI5	0.587[**]
6	MCRC	0.733[**]	DFI	0.656[**]	NDI7	0.671[**]	NDI7	0.546[**]
7	NDI5	0.726[**]	NDI7	0.656[**]	DFI	0.552[**]	DFI	0.498[**]
8	NDTI	0.716[**]	NDTI	0.558[**]	STI	0.498[**]	NDTI	0.444[**]
9	STI	0.709[**]	STI	0.557[**]	NDTI	0.495[**]	STI	0.434[**]
-	SINDRI	0.815[**]	SINDRI	0.790[**]	SINDRI	0.737[**]	SINDRI	0.776[**]
-	CAI	0.869[**]	CAI	0.780[**]	CAI	0.777[**]	CAI	0.580[**]

Note: $\lvert r \rvert$ represent the absolute value of correlation coefficient. [**]. Correlation is significant at the 0.01 level (two-tailed).

Of the eleven indices investigated, the SINDRI leads to the most accurate estimates of CRC (*r* = 0.790) with the wet dataset, whereas the CAI leads to the most accurate estimates of CRC (*r* = 0.869) with the dry dataset. In addition, the SINDRI has an advantage for estimating CRC with various moisture contents because it is significantly more correlated with CRC than are the other broad-band indices or the CAI. Moisture in crop residue impacts the traditional remote-sensing SI-based estimates of CRC except for SINDRI.

Based on the above statistics and analysis of the traditional spectral indices, (i) the hyperspectral CAI, (2) the hyperspectral SINDRI, and (iii) the three best broad-band crop residue SIs (SGNDI, SRNDI, and NDSVI) are chosen for comparison with the proposed CRAI.

4.2. Response of Spectral Indices to Moisture and Soil Background

4.2.1. Response of Spectral Indices to Moisture

Figure 6 shows the six investigated SIs as a function of wheat and maize residue cover (calibration dataset: *n* = 279 for wheat and *n* = 261 for maize) and with various moisture contents. The CRAI increases linearly with wheat residue cover (dry, wet, saturated, and all datasets), whereas the SINDRI is logarithmic in wheat residue cover (Figure 6, wheat). The CAI, SRNDI, NDSVI, and SGNDI are all linearly related to wheat residue cover when using the dry, wet, or saturated datasets. However, this relationship becomes less obvious when using all datasets. The effect of water absorption on the SIs (CAI, SRNDI, NDSVI, and SGNDI) becomes clear as the moisture content of the wheat residue

increases from dry to water saturated. These indices give significantly different results for the dry, wet, and saturated soil and crop residue samples. For example, the SGNDI gives a value of about −0.45 for dry soil, whereas it gives −0.3 and −0.2 for wet and saturated soil, respectively. In addition, it increases from −0.1 to 0 and then to 0.1 for dry, wet, and saturated crop residue. In some extreme cases, the SRNDI, NDSVI, and SGNDI give values for saturated soil that are similar to those for dry wheat residue (Figure 6). The relationship between SIs and CRC for wheat and maize are similar (see Figures 6 and 7, wheat and maize). The correlation coefficients for all datasets (Figure 7, saturated, wet, dry, and all datasets) show that, for strongly varying moisture content, the proposed CRAI may leads to more accurate estimates of the CRC. Thus, the proposed CRAI may help to provide more accurate estimates of CRC.
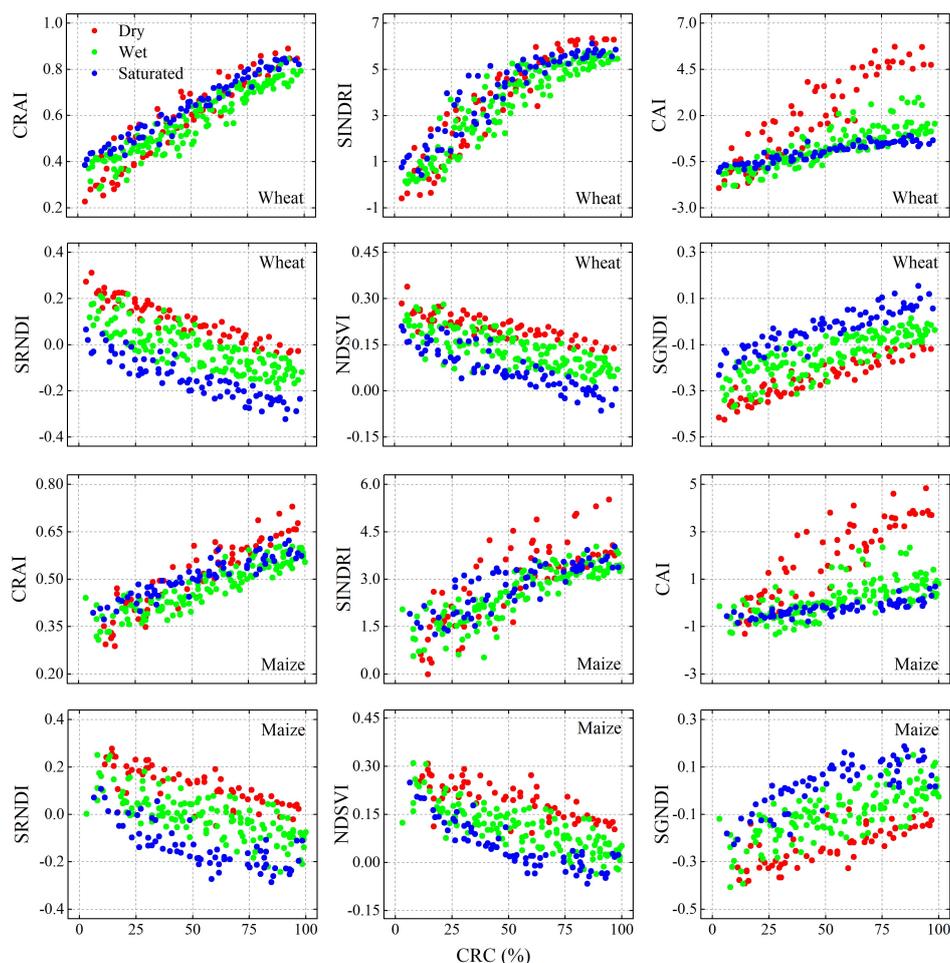
Figure 6. Correlation between spectral indices and crop residue cover for various crop residue moisture contents (laboratory-based calibration dataset: n = 279 for wheat and n = 261 for maize). **Note:** All laboratory-based calibration datasets were divided into three moisture groups (dry, wet, and saturated), and each groups includes four soils (paddy soil, black soil, meadow soil, and brown soil).

4.2.2. Response of Spectral Indices to Soil Background

Figure 8 shows the correlation of the six SIs investigated in this work with winter-wheat CRC for various soil backgrounds and with a single SM content (dry and saturated samples of calibration dataset: n = 137 for wheat). For the four soil backgrounds, the spectral indices and maize residue cover are similarly related (see Figure 8). The CRAI increases linearly with wheat residue cover (brown soil, black soil, meadow soil, paddy soil, and all soils), whereas the SINDRI is logarithmic in wheat residue cover (see Figure 8).
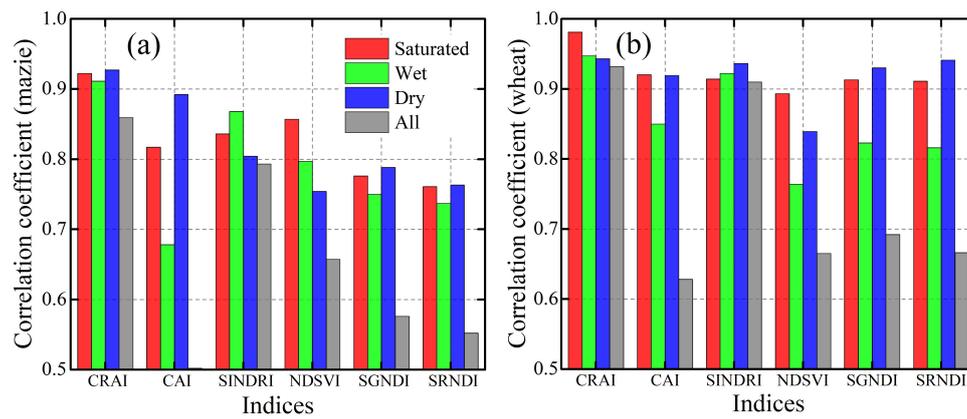
Figure 7. Absolute value of correlation coefficient between: (i) CRC and (ii) CRAI, CAI, SINDRI, NDSVI, SGNDI, and SRNDI for the different datasets for maize (**a**) and wheat (**b**) (see legend).
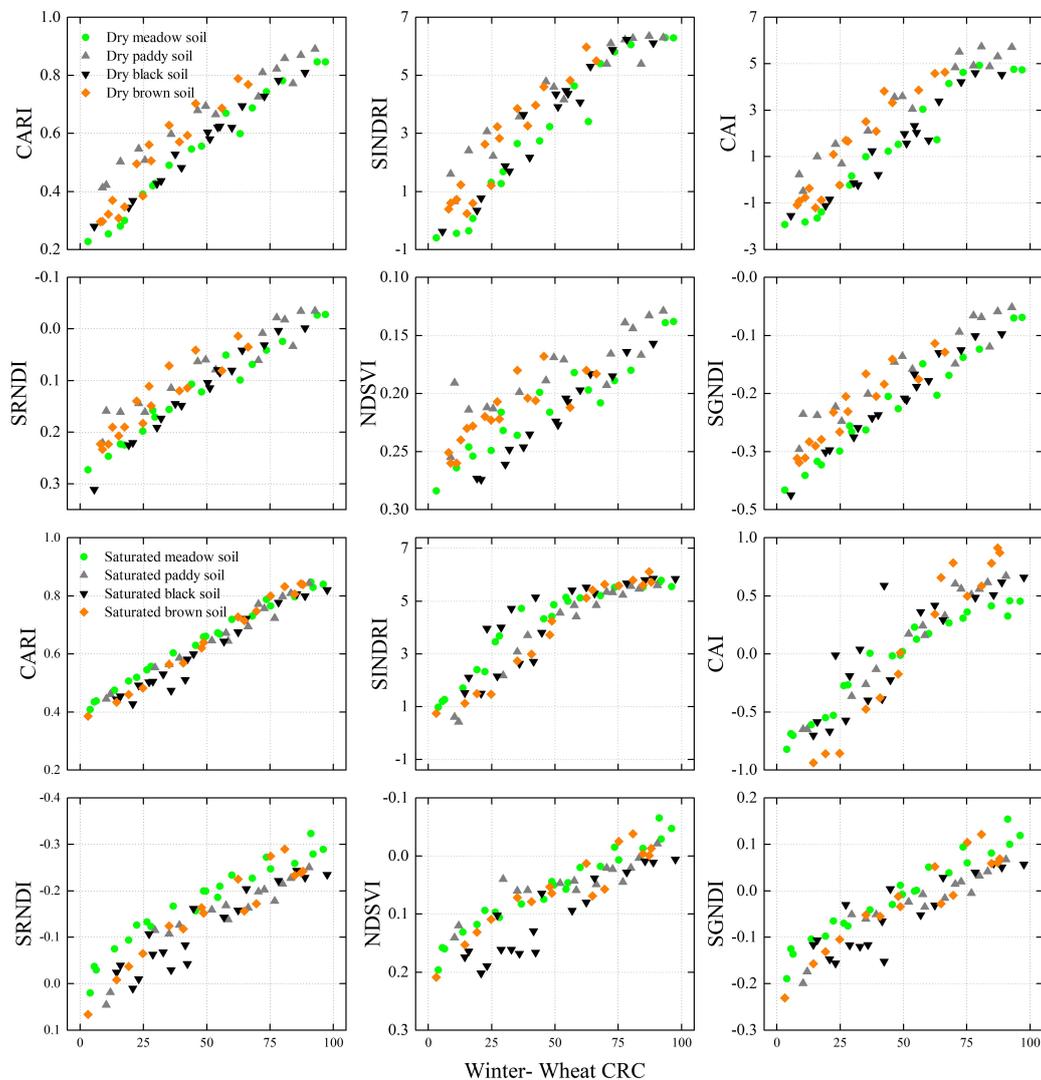
Figure 8. Correlation between spectral indices and winter-wheat CRC for four soil backgrounds at single moisture contents. **Note:** For visualization, the ordinate of the six SIs may differ. Only dry and saturated samples of the calibration dataset were used (*n* = 137), and the data were divided into four soil groups (paddy soil, black soil, meadow soil, and brown soil).

Figure 8 shows the effect of soil background by comparing SIs with CRCs at single moisture contents. Figure 9 gives the absolute value (|r|) of the correlation coefficients between: (i) CRC and (ii) CRAI, CAI, SINDRI, NDSVI, SGNDI, and SRNDI for the different datasets. Figure 9 shows that the soil background (see Figure 9, four soil datasets) has a less-detrimental effect on the remote-sensing-based estimates of CRC than does the moisture content (see Figure 7, all datasets). Overall, both soil background and moisture content have an uncertain effect on the broad-band SIs and the resulting CAI-based estimates of CRC. In other words, it is difficult to estimate CRC from different soils, various SM/CRM using broad-band SIs and CAI (see Figure 7).
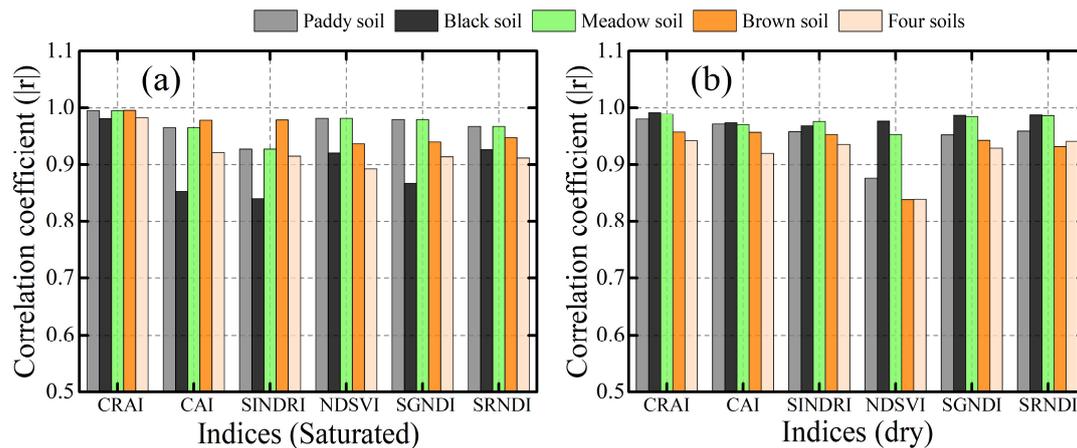
Figure 9. Absolute value (|r|) of correlation coefficient between: (i) CRC and (ii) CRAI, CAI, SINDRI, NDSVI, SGNDI, and SRNDI for saturated (**a**) and dry (**b**) datasets (see legend).

Because the samples in fact contain a variety of samples (dry, wet, and saturated), SIs from a given soil background (see CAI, NDSVI, SGNDI, SRNDI in Figure 7) are less correlated with CRC than are SIs from a given moisture category (see CAI, NDSVI, SGNDI, SRNDI in Figure 9). Mitigating the uncertain effect caused by moisture is of significant importance to properly estimate CRC using remote-sensing techniques.

4.3. Estimation of Crop Residue Cover

We use a linear model (CRC = a × Index + b) in this study to estimate the wheat and maize CRC (see Section 3.2.1. Estimate of Crop Residue Cover). Figures 6 and 8 show the calibration dataset (calibration dataset: $n = 279$ for wheat and $n = 261$ for maize) and Table A4 lists the corresponding estimates of CRC from the linear model. The scatter plots in Figure 9 show the relationships (see linear fits) between the estimated and measured wheat and maize CRC. Table A4 lists the accuracy of the estimates of CRC [MAE (%), RMSE (%), nRMSE (%), and R^2] based on linear models of: (i) the proposed CRAI (ii) the CAI, (iii) SINDRI, and (iv) selected broad-band SIs. Note that, when using different equations (linear versus exponential equations; see Table A4 in the Appendix A), the performance of the SINDRI varies for estimating the CRC. The exponential equation for estimating winter-wheat CRC provides better results than the linear equation, but the opposite holds for estimating the maize CRC.

As shown in Figure 10, CRM affects the estimation of broad-band CRC. For example, with wheat CRC, the lower saturated and wet CRCs are overestimated when using the SRNDI (see Figure 10), whereas the higher wet and dry CRCs are underestimated (Figure 10). The response of the NSDVI and SGNDI to CRM is similar with SRNDI (Figure 10). In this study, dry CRC is overestimated when using the CAI, whereas saturated CRC is underestimated because the CAI decreases with increasing CRM (Figure 6; [20,23]). In addition, the SINDRI may also lead to underestimating the higher wheat CRC (Figure 10). In this work, estimates of CRC based on the CRAI and laboratory-based validation dataset gives the best linear fit for wheat: $y = 0.864x + 7.113$ (MAE = 7.80%, RMSE = 9.54%, nRMSE = 10.46%,

and $R^2 = 0.872$) and for maize $y = 0.743x + 13.174$ (MAE = 11.14%, RMSE = 13.90%, nRMSE = 14.85%, and $R^2 = 0.730$).
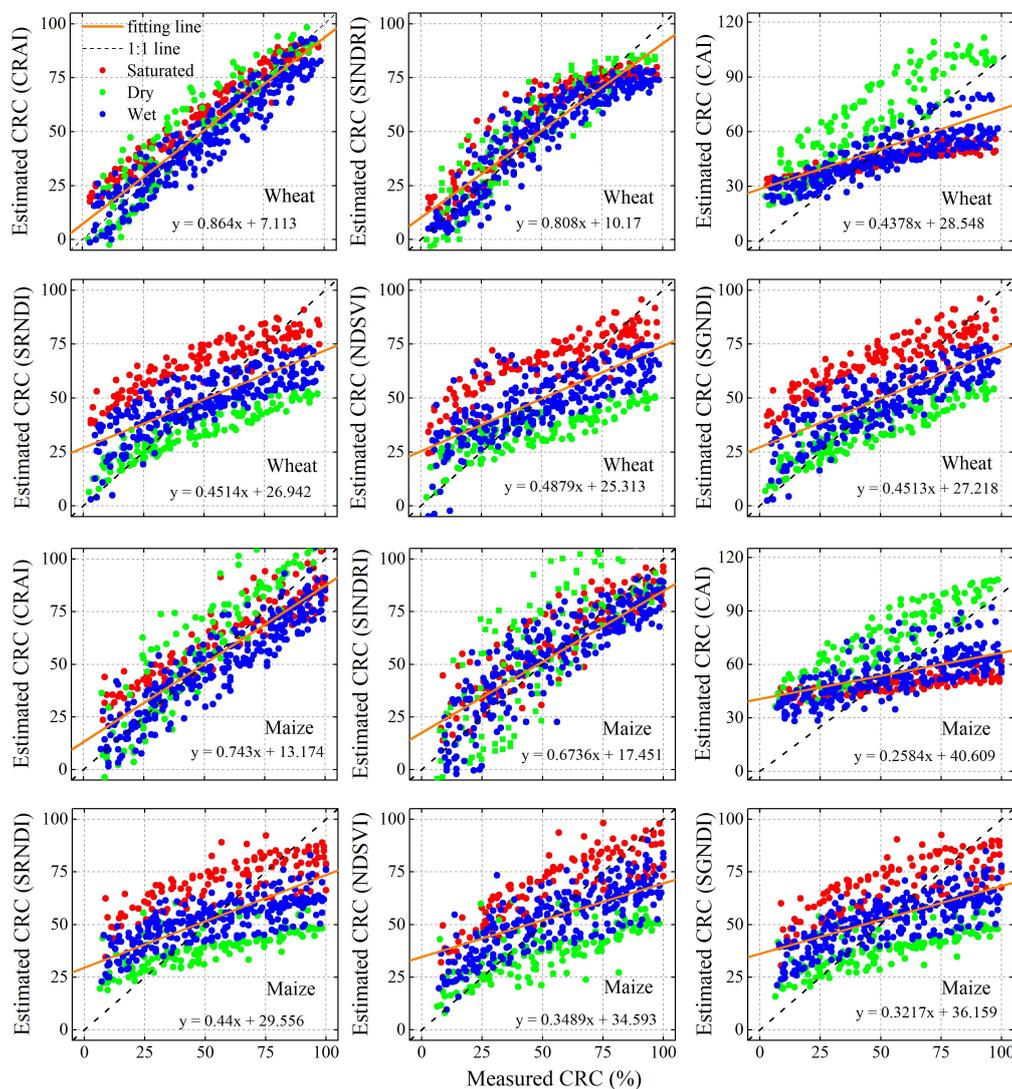
Figure 10. Correlation between estimated and measured CRC (validation dataset: $n = 556$ for wheat and $n = 522$ for maize, formula $y = a \times x + b$ represent the fit line).

5. Analysis and Discussion

5.1. Analysis of Spectral Indices for Crop Residue Cover Using Laboratory Dataset

In this study, the CRC estimation performance of CRAI and 11 selected indices was validate by using a laboratory-based dataset ((i) a dry dataset (air-dried soils and crop residues, n = 392), (ii) a wet dataset (wet soils and crop residues, n = 822), (iii) a saturated dataset (saturated soils and crop residues, n = 402), and (iv) all datasets (n = 1616)). The correlation coefficients between the 11 selected indices and CRC from the laboratory-based dry dataset range from 0.709 to 0.869, so all SIs are strong candidates for estimating CRC (Table 3) from dry samples of soil and crop residue. However, moisture produces an uncertain effect on estimates of CRC based on remote sensing of the selected indices, which significantly reduces the correlation coefficient between the broad-band SIs and CRC from all (dry, wet, saturated) samples (Figures 6, 7 and 10). The laboratory-based results indicate that broad-band SIs do not provide accurate estimates of CRC (see SRNDI, SGNDI, and NDSVI in Figures 10 and 11) when SM/CRM varies significantly.
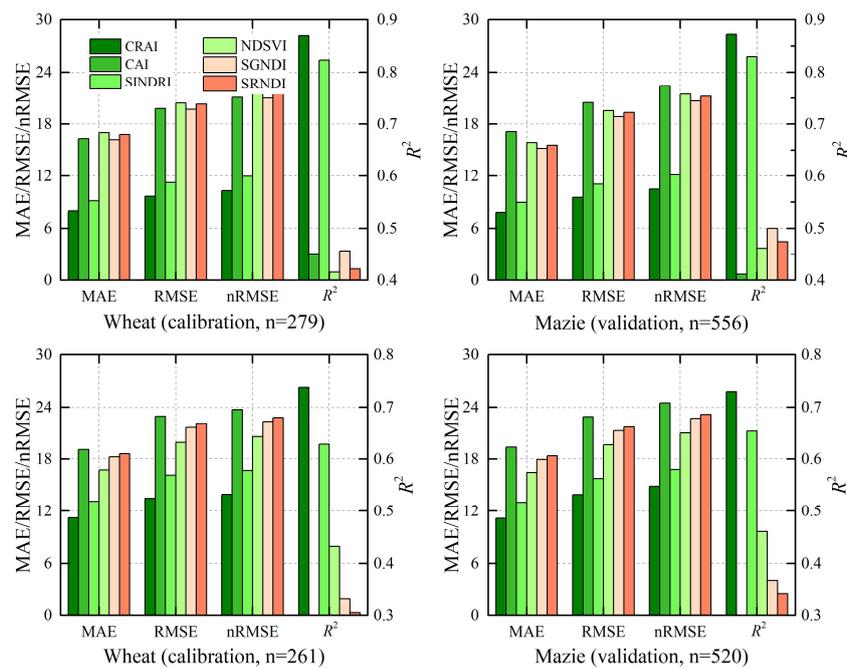
Figure 11. Statistics of regression accuracy (mean absolute error (MAE) (%), root mean square error (RMSE) (%), normalized root mean square error (nRMSE) (%), and coefficient of determination (R^2)).

Figures 10 and 11 show that, compared with the three investigated broad-band indices and the CAI, the SINDRI offers an advantage for estimating CRC with various soil backgrounds and moisture contents. However, previous studies indicate that the water and soil background affects the SINDRI [24]. Quemada et al. [24,40] suggest that the use of a water index to correct the reflectance of each spectral band substantially mitigates the uncertain effects of moisture on CRC estimates. However, correcting for moisture by using a water index requires prior field knowledge (e.g., SM/CRM response to water index, see [24,40]). More importantly, the moisture-correction parameters may differ for the different soils and crop residues. Therefore, applying a water index to correct for moisture may be of limited use in practice. According to our preceding analysis (Section 4.1, Table 3), the CAI gives the best estimate of CRC (r = 0.869) for the dry dataset. However, the CAI leads to poor estimates for samples with greater water content (Table 3, Figures 6–11). The main problem is that the CAI for pure crop residue diminishes rapidly with increasing moisture (Figure 6), which indicates that CRM reduces the accuracy of CRC estimates based on the CAI. A more detailed analysis of the CAI of crop residues and soils as a function of CRM is available in the literature [20,23,24].

In practice, the water content of soil and crop residue often varies spatially due to minor changes in local topography, rainfall, and irrigation. In addition, different soils often have significantly different spectra (Figure 1). In this study, the proposed CRAI uses two angles to estimate CRC, with the angle β involving the same three bands as the CAI (2031, 2011, and 2201 nm), and the angle α (involving bands at 833 and 1670 nm) correcting for moisture. The proposed CRAI accurately estimates the CRC regardless of soil, soil moisture, or crop residue moisture. Of course, the results (Figures 10 and 11) and corresponding analysis comes from a laboratory-based dataset.

5.2. Limitations and Future Application of Laboratory-Based CRAI

This work uses four spectrally distinct soils (paddy soil, black soil, meadow soil, and brown soil; see Figure 1), two crop residues (winter wheat and maize; see Figure 2), and four levels of SM/CRM to produce a reliable representation of the actual conditions in the field (Table 2). The use of laboratory-based mixed hyperspectral data with varying moisture content allows us to focus on how the soil and crop residue hyperspectral bands at 833, 1670, 2031, 2101, and 2201 nm respond to moisture

and soil background, and thereby to propose the CRAI. Laboratory-based mixed hyperspectral data from a total of 1616 sets of residue and soil (wheat: 835 for wheat and 781 for maize) with varying moisture content were used to verify the proposed CRAI. However, CRAI is confined by only a laboratory-based dataset. For the moment, CRAI was limited because it has yet to be verified in the field, and require additional real satellite-based hyperspectral remote sensing testing. Eventually, the usefulness of this study is its future application of the new proposed index to satellites and other remote sensors.

Furthermore, despite the simple calculation and the high accuracy of the CRC estimate, the proposed method may have limited applicability for the moment. The main problem is the difficulty of obtaining hyperspectral images, which makes it difficult to use the proposed CRAI for estimating large-scale CRC. In recent years, hyperspectral remote-sensing data acquired from the ground (field and laboratory) [5,18,36,41,49,50], unmanned aerial vehicles and airborne platforms (Airborne Visible/Infrared Imaging Spectrometer-Next Generation (AVIRIS-NG) [51], Headwall Photonics Hyper-spec VNIR-SWIR Dual-sensor), and satellite platforms (EO-1 Hyperion [17,52], Compact High Resolution Imaging Spectrometer (CHRIS) proba-1 [53]) have been able to capture field spectra in narrow bands, thereby, the method can be applied. Of course, numerous other hyperspectral-based CRC estimation methods exist, and many fruitful results have been achieved [17,39,52]. Note, that the number of satellite-based hyperspectral sensors is rising due to this growing demand, examples include: the Advanced Hyper-Spectral Imager (AHSI) mounted on GF-5 of China [launched on May 9, 2018; spectral resolution: 0.4~0.9 μm (5 nm), 0.9~2.5 μm (10 nm); ground spatial resolution: 30 m [54]] and the German Environmental Mapping and Analysis Program (EnMAP) mission (EnMAP, 2019). In addition, the feasibility of estimating CRC in the field by using the CRAI from hyperspectral images should be determined by additional field tests. However, field validation can only be perform when GF-5 AHSI is ready for providing hyperspectral images of harvested farmland and currently, it has not yet been undertaken. Thus, further studies are required to verify the use of satellite hyperspectral remote-sensing images for different crops and ecological areas. In addition, because numerous broadband remote-sensing data are free and available, a multispectral crop residue angle index will be more valuable than the hyperspectral version presented herein. Thus, the response to moisture and soil background of broadband remote-sensing multispectral imaging requires additional analysis, which means that further studies are also required to develop a multispectral version of the CRC angle index.

6. Conclusions

Based on the large quantities of laboratory-based hyperspectral dataset, this study proposes a crop residue angle index (CRAI) for estimating CRC based on five bands (833, 1670, 2031, 2101, and 2201 nm). We measured laboratory-based mixed hyperspectral reflectance from two crop residues (wheat and maize) and from four spectrally distinct soils (paddy soil, black soil, meadow soil, and brown soil) and included dry, wet, and saturated samples (Table 2). We compared how moisture content and soil background affected the selected spectral indices (SIs) ((i) the proposed CRAI, (ii) the CAI, (iii) the SINDRI, and (iv) selected broad-band Sis) by using laboratory-based datasets containing: (i) air-dried soils and crop residues, (ii) wet soils and crop residues, (iii) saturated soils and crop residues, and (iv) all datasets ((i)–(iii)). The main conclusions of this work are as follows:

(i)　Mitigating the uncertain effect caused by moisture is of significant importance to properly estimate CRC using remote-sensing techniques. Crop residue moisture content significantly affects the traditional SIs (Table 3, Figure 6) except for SINDRI. All broad-band indices are less correlated with CRC when using all datasets than when using only the dry, wet, or saturated dataset (Table 3). Although the CAI provides the best estimate of CRC ($r = 0.869$) when using the dry dataset, it leads to a poor estimate of CRC ($r = 0.580$) when crop residue samples have varying moisture content (Table 3).

(ii)　In this work, the proposed CRAI accurately estimates the CRC regardless of soil, soil moisture, or crop residue moisture by using a laboratory-based dataset (Table 2). The CRAI combines

two features that reflect the moisture content in soil and crop residue. The first is the different reflectance of soil and crop residue as a function of moisture in the near-infrared band (833 nm) and short-wave near-infrared band (1670 nm), and the second is different reflectance of soils and crop residues to lignin, cellulose, and moisture in the bands at 2101, 2031, and 2201 nm. However, note that the CRAI has yet to be verified in the field. Thus, above-mentioned advantages of new proposed index require additional real satellite-based hyperspectral remote sensing testing.

(iii) The current study uses laboratory-based tests, which allows us to compare samples with different moisture content ((i) dry, (ii) wet, (iii) saturated, and (iv) all datasets). To confirm that the findings apply to a broader range of crops and ecological areas, additional field-based experiments are planned.

(iv) Because numerous broadband remote-sensing data are free and available, a multispectral crop residue angle index will be more valuable than the hyperspectral version presented herein. Therefore, broad-band multi-spectral reflectance respond to SM/CRM should be analyzed in future works.

Appendix A

The summary of field soil characteristics is presented in Table A1. The details numbers in Figures 7, 9 and 11 are shown in Tables A2–A4. The performance of SINDRI-based CRC estimates made with an exponential equation are also shown in Table A4 of the Appendix A.

Table A1. Summary of characteristics four soils.

Soil Name	City	Color	Soil Order	Clay [a]	Silt [b]	Sand [c]	Soil Type	PH
Paddy Soil	Nanjing	10YR4/3	Anthrosols	99.95%	0.05%	0.00%	Clay	6.46
Black Soil	Jining	10YR4/3	Vertisols	87.00%	6.83%	6.17%	Clay	7.36
Meadow Soil	Jining	2.5YR7/4	Histosols	76.7%	20.4%	2.90%	Clay	7.74
Brown Soil	Jining	2.5YR6/3	Alfisols	71.10%	11.70%	17.20%	Clay	6.54

[a] Particle size (< 0.002 mm), [b] Particle size (0.002-0.05 mm), [c] Particle size (0.05-2 mm).

Table A2. Absolute value of correlation coefficient.

Types	Indices	Saturated	Wet	Dry	All
Wheat	CRAI	0.981	0.947	0.943	0.932
	CAI	0.920	0.850	0.919	0.628
	SINDRI	0.914	0.922	0.936	0.910
	NDSVI	0.893	0.764	0.839	0.665
	SGNDI	0.913	0.823	0.930	0.692
	SRNDI	0.911	0.816	0.941	0.666
Maize	CRAI	0.922	0.911	0.927	0.859
	CAI	0.817	0.678	0.892	0.502
	SINDRI	0.836	0.868	0.804	0.793
	NDSVI	0.857	0.797	0.754	0.657
	SGNDI	0.776	0.750	0.788	0.576
	SRNDI	0.761	0.737	0.763	0.552

Table A3. Absolute value of correlation coefficient.

Types	Indices	Paddy Soil	Black Soil	Meadow Soil	Brown Soil	Four Soils
	CRAI	0.979	0.992	0.989	0.957	0.943
	CAI	0.971	0.973	0.970	0.957	0.919
Dry	SINDRI	0.958	0.968	0.975	0.953	0.936
	NDSVI	0.877	0.976	0.953	0.838	0.839
	SGNDI	0.953	0.986	0.984	0.943	0.930
	SRNDI	0.959	0.986	0.985	0.932	0.941
	CRAI	0.995	0.980	0.995	0.996	0.981
	CAI	0.965	0.852	0.965	0.977	0.920
Saturated	SINDRI	0.928	0.840	0.928	0.978	0.914
	NDSVI	0.980	0.920	0.980	0.937	0.893
	SGNDI	0.978	0.868	0.978	0.940	0.913
	SRNDI	0.967	0.927	0.967	0.948	0.911

Table A4. Descriptive statistics of regression accuracy [MAE (%), RMSE (%), nRMSE (%), and R^2].

Crops	Indices	Calibration (279 Wheat and 261 Maize)					Validation (556 Wheat and 520 Maize)			
		Regression Model	MAE	RMSE	nRMSE	R^2	MAE	RMSE	nRMSE	R^2
	CRAI	$y = 159.52\,x - 43.67$	7.99	9.64	10.28	0.870	7.80	9.54	10.46	0.872
	CAI	$y = 11.98\,x + 43.14$	16.30	19.80	21.11	0.451	17.13	20.49	22.47	0.411
	SINDRI (l)	$y = 12.74\,x + 4.54$	9.15	11.22	11.97	0.824	8.95	11.03	12.10	0.830
Wheat	SINDRI (e)	$y = 11.57 \exp(0.35\,x)$	8.59	10.86	11.50	0.842	8.53	10.64	11.10	0.846
	NDSVI	$y = -223.99\,x + 81.10$	17.02	20.43	21.78	0.416	15.85	19.56	21.45	0.462
	SGNDI	$y = 152.47\,x + 72.55$	16.20	19.70	21.00	0.457	15.19	18.87	20.69	0.500
	SRNDI	$y = -131.65\,x + 48.31$	16.81	20.32	21.66	0.422	15.57	19.35	21.22	0.474
	CRAI	$y = 271.1\,x - 78.63$	11.21	13.48	13.93	0.738	11.14	13.90	14.85	0.730
	CAI	$y = 10.53\,x + 49.65$	19.10	22.96	23.72	0.252	19.36	22.93	24.49	0.260
	SINDRI (l)	$y = 21.60\,x - 3.69$	13.09	16.13	16.66	0.629	12.99	15.73	16.81	0.654
Maize	SINDRI (e)	$y = 11.73 \exp(0.51\,x)$	14.79	20.38	21.10	0.498	14.43	19.97	21.30	0.526
	NDSVI	$y = -208.59\,x + 78.12$	16.75	19.92	20.58	0.432	16.43	19.65	21.00	0.461
	SGNDI	$y = 112.82\,x + 65.70$	18.26	21.65	22.37	0.331	17.96	21.27	22.73	0.368
	SRNDI	$y = -115.69\,x + 53.40$	18.61	22.08	22.81	0.305	18.36	21.71	23.20	0.341

Note: SINDRI (l) and SINDRI (e) represent SINDRI-based estimates of CRC made by using the linear and exponential equations.

References

1. Mu, X.; Zhao, Y.; Liu, K.; Ji, B.; Guo, H.; Xue, Z.; Li, C. Responses of soil properties, root growth and crop yield to tillage and crop residue management in a wheat-maize cropping system on the North China Plain. *Eur. J. Agron.* **2016**, *78*, 32–43. [CrossRef]

2. Kimble, J.M.; Follett, R.F.; Cole, C.V. *The Potential of US Cropland to Sequester Carbon and Mitigate the Greenhouse Effect*; CRC Press: Boca Raton, FL, USA, 1998; ISBN 157504112X.

3. Erenstein, O. Crop residue mulching in tropical and semi-tropical countries: An evaluation of residue availability and other technological implications. *Soil Tillage Res.* **2002**, *67*, 115–133. [CrossRef]

4. Lal, R.; Bruce, J.P. The potential of world cropland soils to sequester C and mitigate the greenhouse effect. *Environ. Sci. Policy* **1999**. [CrossRef]

5. Daughtry, C.S.T.; Serbin, G.; Reeves, J.B.; Doraiswamy, P.C.; Hunt, E.R. Spectral reflectance of wheat residue during decomposition and remotely sensed estimates of residue cover. *Remote Sens.* **2010**, *2*, 416–431. [CrossRef]

6. Zhang, T.; Wooster, M.J.; Xu, W. Remote Sensing of Environment Approaches for synergistically exploiting VIIRS I- and M-Band data in regional active fi re detection and FRP assessment: A demonstration with respect to agricultural residue burning in Eastern China. *Remote Sens. Environ.* **2017**, *198*, 407–424. [CrossRef]

7. Chen, S.; Xu, C.; Yan, J.; Zhang, X.; Zhang, X.; Wang, D. The influence of the type of crop residue on soil organic carbon fractions: An 11-year field study of rice-based cropping systems in southeast China. *Agric. Ecosyst. Environ.* **2016**, *223*, 261–269. [CrossRef]

8. Eriksen-Hamel, N.S.; Speratti, A.B.; Whalen, J.K.; Légère, A.; Madramootoo, C.A. Earthworm populations and growth rates related to long-term crop residue and tillage management. *Soil Tillage Res.* **2009**, *104*, 311–316. [CrossRef]

9. Morrison, J.E.; Lemunyon, J.; Bogusch, H.C. Sources of variation and performance of 9 devices when measuring percent residue cover. *Trans. ASAE* **1995**, *38*, 521–529. [CrossRef]

10. Morrison, J.E.; Huang, C.-H.; Lightle, D.T.; Daughty, C.S.T. Residue measurement techniques. *J. Soil Water Conserv.* **1993**, *48*, 478–483.

11. Li, Z.; Guo, X. Non-photosynthetic vegetation biomass estimation in semiarid Canadian mixed grasslands using ground hyperspectral data, Landsat 8 OLI, and Sentinel-2 images. *Int. J. Remote Sens.* **2018**, *39*, 6893–6913. [CrossRef]

12. Hamidisepehr, A.; Sama, M.P.; Turner, A.P.; Wendroth, O.O. A Method for Reflectance Index Wavelength Selection from Moisture-Controlled Soil and Crop Residue Samples. *Trans. ASABE* **2017**, *60*, 1479–1487. [CrossRef]

13. Hill, M.J.; Román, M.O.; Schaaf, C.B. Dynamics of vegetation indices in tropical and subtropical savannas defined by ecoregions and Moderate Resolution Imaging Spectroradiometer (MODIS) land cover. *Geocarto Int.* **2012**, *27*, 153–191. [CrossRef]

14. Hively, W.D.; Lamb, B.T.; Daughtry, C.S.T.; Shermeyer, J.; McCarty, G.W.; Quemada, M. Mapping crop residue and tillage intensity using WorldView-3 satellite shortwave infrared residue indices. *Remote Sens.* **2018**, *10*, 1657. [CrossRef]

15. Ridd, M.K. Exploring a V-I-S (Vegetation-impervious surface-soil) model for urban ecosystem analysis through remote sensing: Comparative anatomy for citiest. *Int. J. Remote Sens.* **1995**, *16*, 2165–2185. [CrossRef]

16. Wu, M.; Wang, J.; Wang, G.; Zou, X.; Wang, Z.; Chai, G. Estimating the fractional cover of photosynthetic vegetation, non-photosynthetic vegetation and bare soil from MODIS data: Assessing the applicability of the NDVI-DFI model in the typical Xilingol grasslands. *Int. J. Appl. Earth Obs. Geoinf.* **2019**, *76*, 154–166. [CrossRef]

17. Sonmez, N.K.; Slater, B. Measuring intensity of tillage and plant residue cover using remote sensing. *Eur. J. Remote Sens.* **2016**, *49*, 121–135. [CrossRef]

18. Wang, C.K.; Pan, X.Z.; Liu, Y.; Li, Y.L.; Shi, R.J.; Zhou, R.; Xie, X.L. Alleviating moisture effects on remote sensing estimation of crop residue cover. *Agron. J.* **2013**, *105*, 967–976. [CrossRef]

19. Daughtry, C.S.; Beeson, P.C.; Milak, S.; Akhmedov, B.; Sadeghi, A.M.; Hunt, E.R.; Tomer, M.D. Assessing the extent of conservation tillage in agricultural landscapes. In Proceedings of the Remote Sensing for Agriculture, Ecosystems, and Hydrology XIV, Edinburgh, Scotland, 24–26 September 2012; Volume 8531. [CrossRef]

20. Daughtry, C.S.T. Discriminating crop residues from soil by shortwave infrared reflectance. *Agron. J.* **2001**, *93*, 125–131. [CrossRef]

21. Wang, C. *Estimation of Crop Residue Cover by Remote Rensing and Correction of Moisture Effects on Estimates*; University of Chinese Academy of Sciences: Beijing, China, 2013.

22. Daughtry, C.S.T.; Hunt, E.R. Mitigating the effects of soil and residue water contents on remotely sensed estimates of crop residue cover. *Remote Sens. Environ.* **2008**, *112*, 1647–1657. [CrossRef]

23. Wang, C.; Pan, X.; Liu, Y.; Li, Y.; Zhou, R.; Xie, X. Modeling the Effect of Moisture on the Reflectance of Crop Residues. *Agron. J.* **2012**, *104*, 1652–1657. [CrossRef]

24. Quemada, M.; Daughtry, C.S.T. Spectral indices to improve crop residue cover estimation under varying moisture conditions. *Remote Sens.* **2016**, *8*, 660. [CrossRef]

25. Serbin, G.; Daughtry, C.S.T.; Hunt, E.R.; Brown, D.J.; McCarty, G.W. Effect of Soil Spectral Properties on Remote Sensing of Crop Residue Cover. *Soil Sci. Soc. Am. J.* **2009**, *73*, 1545–1558. [CrossRef]

26. Serbin, G.; Daughtry, C.S.T.; Hunt, E.R.; Reeves, J.B.; Brown, D.J. Remote Sensing of Environment Effects of soil composition and mineralogy on remote sensing of crop residue cover. *Remote Sens. Environ.* **2009**, *113*, 224–238. [CrossRef]

27. Omar, Z.; Stathaki, T. Hyperspectral unmixing overview: Geometrical, statistical, and sparse regression-based approaches. *IEEE J. Sel. Top. Appl. Earth Obs. Remote Sens.* **2012**, *5*, 354–379. [CrossRef]

28. Bateson, A.; Curtis, B. A method for manual endmembers selection and spectral unmixing. *Remote Sens. Environ.* **1996**, *55*, 229–243. [CrossRef]

29. Pacheco, A.; McNairn, H. Evaluating multispectral remote sensing and spectral unmixing analysis for crop residue mapping. *Remote Sens. Environ.* **2010**, *114*, 2219–2228. [CrossRef]

30. Cao, X.; Chen, J.; Matsushita, B.; Imura, H. Developing a MODIS-based index to discriminate dead fuel from photosynthetic vegetation and soil background in the Asian steppe area. *Int. J. Remote Sens.* **2010**, *31*, 1589–1604. [CrossRef]

31. Mcnairn, H.; Protz, R. Mapping corn residue cover on agricultural fields in oxford county, ontario, using thematic mapper. *Can. J. Remote Sens.* **1993**, *19*, 152–159. [CrossRef]

32. Van Deventer, A.P.; Ward, A.D.; Gowda, P.M.H.M.; Lyon, J.G. Using thematic mapper data to identify contrasting soil plains and tillage practices. *Photogramm. Eng. Remote Sens.* **1997**, *63*, 87–93. [CrossRef]

33. Qi, J.; Marsett, R.; Heilman, P.; Bieden-bender, S.; Moran, S.; Goodrich, D.; Weltz, M. Ranges improves satellite-based information and land cover assessments in southwest United States. *Eos Trans. Am. Geophys. Union* **2002**, *83*. [CrossRef]

34. Jin, X.; Ma, J.; Wen, Z.; Song, K. Estimation of maize residue cover using Landsat-8 OLI image spectral information and textural features. *Remote Sens.* **2015**, *7*, 14559–14575. [CrossRef]

35. Daughtry, C.S.T.; McMurtrey, J.E.; Chappelle, E.W.; Hunter, W.J.; Steiner, J.L. Measuring crop residue cover using remote sensing techniques. *Theor. Appl. Climatol.* **1996**, *54*, 17–26. [CrossRef]

36. Serbin, G.; Hunt, E.R.; Daughtry, C.S.T.; McCarty, G.W.; Doraiswamy, P.C. An improved ASTER index for remote sensing of crop residue. *Remote Sens.* **2009**, *1*, 971–991. [CrossRef]

37. Daughtry, C.S.T.; Hunt, E.R.; Doraiswamy, P.C.; McMurtrey, J.E. Remote sensing the spatial distribution of crop residues. *Agron. J.* **2005**, *97*, 864–871. [CrossRef]

38. Biard, F.; Baret, F. Crop residue estimation using multiband reflectance. *Remote Sens. Environ.* **1997**, *59*, 530–536. [CrossRef]

39. Guerschman, J.P.; Hill, M.J.; Renzullo, L.J.; Barrett, D.J.; Marks, A.S.; Botha, E.J. Estimating fractional cover of photosynthetic vegetation, non-photosynthetic vegetation and bare soil in the Australian tropical savanna region upscaling the EO-1 Hyperion and MODIS sensors. *Remote Sens. Environ.* **2009**, *113*, 928–945. [CrossRef]

40. Quemada, M.; Hively, W.D.; Daughtry, C.S.T.; Lamb, B.T.; Shermeyer, J. Improved crop residue cover estimates obtained by coupling spectral indices for residue and moisture. *Remote Sens. Environ.* **2018**, *206*, 33–44. [CrossRef]

41. Yue, J.; Tian, Q.; Tang, S.; Xu, K.; Zhou, C. A dynamic soil endmember spectrum selection approach for soil and crop residue linear spectral unmixing analysis. *Int. J. Appl. Earth Obs. Geoinf.* **2019**, *78*, 306–317. [CrossRef]

42. Jacquemoud, S.; Baret, F.; Hanocq, J.F. Modeling spectral and bidirectional soil reflectance. *Remote Sens. Environ.* **1992**, *41*, 123–132. [CrossRef]

43. Galvão, L.S.; Vitorello, Í. Variability of laboratory measured soil lines of soils from southeastern Brazil. *Remote Sens. Environ.* **1998**, *63*, 166–181. [CrossRef]

44. Muller, E.; Décamps, H. Modeling soil moisture–reflectance. *Remote Sens. Environ.* **2001**, *76*, 173–180. [CrossRef]

45. Twomey, S.A.; Bohren, C.F.; Merganthaler, J.L. Reflectance and albedo difference between wet and dry surfaces. *Appl. Opt.* **1986**, *25*, 431–437. [CrossRef]

46. Palmer, K.F.; Williams, D. Optical properties of water in the near infrared. *J. Opt. Soc. Am.* **1974**, *64*, 1107–1110. [CrossRef]

47. Nagler, P.L.; Daughtry, C.S.T.; Goward, S.N. Plant litter and soil reflectance. *Remote Sens. Environ.* **2000**, *71*, 207–215. [CrossRef]

48. Sullivan, D.G.; Truman, C.C.; Schomberg, H.H.; Endale, D.M.; Strickland, T.C. Evaluating techniques for determining tillage regime in the Southeastern Coastal Plain and piedmont. *Agron. J.* **2006**, *98*, 1236–1246. [CrossRef]

49. Daughtry, C.S.T.; Hunt, E.R.; McMurtrey, J.E. Assessing crop residue cover using shortwave infrared reflectance. *Remote Sens. Environ.* **2004**, *90*, 126–134. [CrossRef]

50. Nagler, P.L.; Inoue, Y.; Glenn, E.P.; Russ, A.L.; Daughtry, C.S.T. Cellulose absorption index (CAI) to quantify mixed soil-plant litter scenes. *Remote Sens. Environ.* **2003**, *87*, 310–325. [CrossRef]

51. Dashti, H.; Glenn, N.F.; Spaete, L.P.; Ilangakoon, N. *Hyperspectral Imagery from AVIRIS-NG for Sites in ID and CA, USA, 2014 and 2015*; ORNL DAAC: Oak Ridge, TN, USA, 2018. [CrossRef]

52. Bannari, A.; Staenz, K.; Champagne, C.; Khurshid, K.S. Spatial variability mapping of crop residue using hyperion (EO-1) hyperspectral data. *Remote Sens.* **2015**, *7*, 8107–8127. [CrossRef]

53. ESA Compact High Resolution Imaging Spectrometer. Available online: https://earth.esa.int/web/guest/missions/esa-operational-eo-missions/proba (accessed on 25 March 2019).

54. Sun, Y.; Jiang, G.; Yunduan, L.I.; Yang, Y.; Dai, H.; Jun, H.E.; Qinghao, Y.E.; Cao, Q.; Dong, C.; Zhao, S. GF-5 Satellite: Overview and Application Prospects. *Spacecr. Recover. Remote Sens.* **2018**, *39*, 1–13. [CrossRef]